01 Apr 2000

# Solid-State Deuterium Nuclear Magnetic Resonance of the Methyl Dynamics of Poly(Alpha-methylstyrene) and Polymethylphenylsilane

Robert D. O'Connor

Eric J. Ginsburg

Frank D. Blum
*Missouri University of Science and Technology*



## Recommended Citation

R. D. O'Connor et al., "Solid-State Deuterium Nuclear Magnetic Resonance of the Methyl Dynamics of Poly(Alpha-methylstyrene) and Polymethylphenylsilane," *Journal of Chemical Physics*, American Institute of Physics (AIP), Apr 2000.
The definitive version is available at https://doi.org/10.1063/1.481288

# Solid-state deuterium nuclear magnetic resonance of the methyl dynamics of poly($\alpha$-methylstyrene) and polymethylphenylsilane

Robert D. O'Connor[a)]
*Department of Chemistry, University of Missouri–Rolla, Rolla, Missouri 65409-0010*

Eric J. Ginsburg
*IBM Research Division, IBM Almaden Research Center, San Jose, California 95120-6099 and Abbott Laboratories, 97D/AP4, Abbott Park, Illinois 60064-3500*

Frank D. Blum[b)]
*IBM Research Division, IBM Almaden Research Center, San Jose, California 95120-6099 and Department of Chemistry and Materials Research Center, University of Missouri–Rolla, Rolla, Missouri 65409-0010*

(Received 10 August 1999; accepted 1 February 2000)

The methyl-$d_3$ dynamics of two relatively similar polymers, poly($\alpha$-methylstyrene) (PAMS-$d_3$) and polymethylphenylsilane (PMPS-$d_3$), are investigated via deuterium NMR relaxation experiments. Our analysis of the relaxation data uses the entire solid-echo spectra to maximize the precision of the experiments with regard to the information available on the methyl dynamics. The analysis is novel in that it does not use $M_\infty$ or $M_0$ to fit the relaxation data. Additionally, the three-site symmetric jump model is shown to not have an observable azimuthal angular dependence for $T_1$ relaxation. The methyl dynamics are quantified with $\tau_m$, $\sigma$, and $f$ which are the log-average correlation time, half-height full-width (base 10) of a log-normal distribution of reorientation rates, and the anisotropy of the relaxation, respectively. The anisotropy parameter, $f$, is based on a serial combination of the rotational diffusion and symmetric three-site jump reorientation of a methyl deuteron. This serial model coupled with a distribution of $\tau_c$'s has a minimal number of parameters that have physical meaning and quantify the observations of our relaxation data. Generally, at similar temperatures the methyl reorientation in PAMS-$d_3$ is at least 100 times slower than that of PMPS-$d_3$. For both polymers, both $\tau_m$ and $\sigma$ decrease with increasing temperature, resulting in activation energies of 12 and 5 kJ/mol for PAMS-$d_3$ and PMPS-$d_3$, respectively. Also, with increasing temperature a mechanistic change from three-site jump to rotational diffusion is observed and quantified. This information, along with that of other studies, suggests that the PAMS-$d_3$ methyls have highly restrictive environments that may be closely coupled to phenyl-ring reorientation. © *2000 American Institute of Physics.* [S0021-9606(00)50416-4]

## INTRODUCTION

Nuclear magnetic relaxation studies are often used to infer dynamic information about molecular systems. Typically, relatively fast motions with correlation times, $\tau_c$, smaller than $10^{-6}$ s are studied, but slower motions can also be probed.[1,2] Relaxation data is generally interpreted in terms of a model and much research has been done on the formulation of models for various types of molecular motion.[1–12] Many of these models are encompassed in the generalized stochastic model of Lindenberg and Cukier.[4] A different approach is to extract the maximum amount of information from the data into as few parameters as needed.[12] Then, if possible, these parameters can be related to a physical model.

In this study, deuterium relaxation is used to probe the solid-state methyl dynamics of poly($\alpha$-methylstyrene)-$d_3$ (PAMS-$d_3$) and polymethylphenylsilane-$d_3$ (PMPS-$d_3$). Many reviews are available on the subject of deuterium relaxation.[13–16] The analysis of this study uses relationships that are independent of some of the experimental parameters that typically limit the precision of relaxation data. Also, by incorporating the methyl relaxation formalism of Torchia and Szabo[3] with the exponential nature of relaxation, a few modifications and simplifications of methyl relaxation are derived. Though a model is used, the analysis is similar to the model-free approach of Lipari and Szabo[12] in that its first goal is to quantify the essential features of solid-state polymer relaxation data which are the reorientation rate, nonexponential relaxation, and anisotropy. Finally, with the aid of other information, the results are related to differences between what appear to be two relatively similar systems.

## THEORY

Molecular motion induces nuclear spin relaxation by causing fluctuations in local fields (couplings) that result in energy level transitions. For a deuteron, the coupling of the nuclear quadrupole moment to the electric field gradient (efg) of the bond is primarily responsible for relaxation.[17] This coupling depends on the relative orientation of the efg

[a)]Present address: Department of Chemistry, Washington University, St. Louis, Missouri 63130.
[b)]Author to whom correspondence should be addressed; University of Missouri–Rolla. Electronic mail: fblum@umr.edu

 

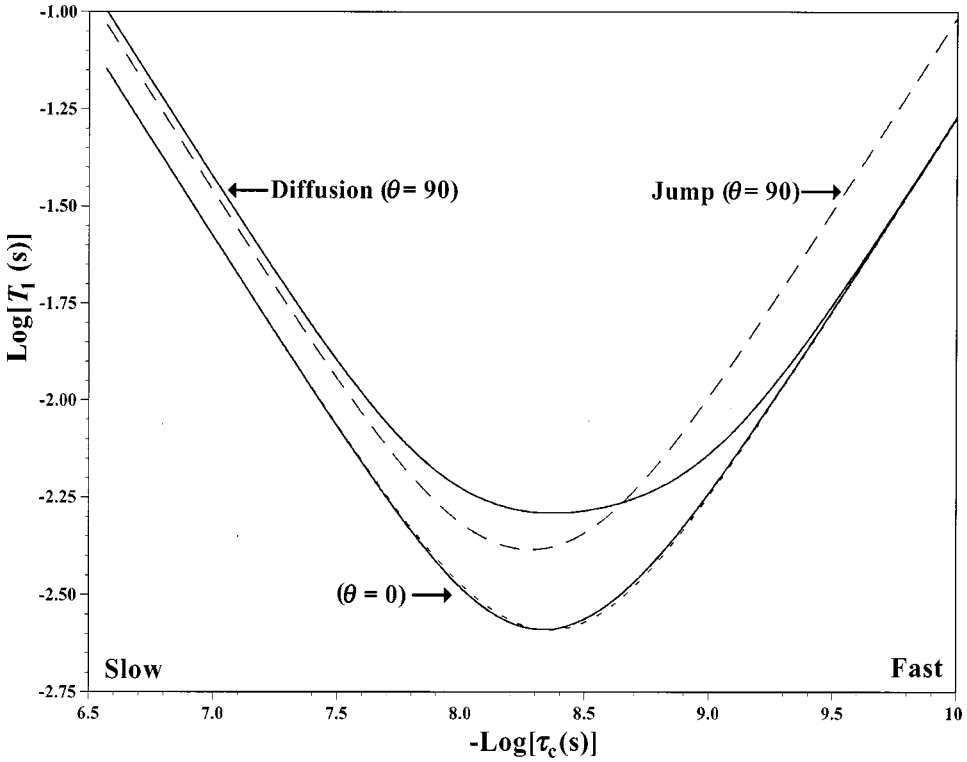


FIG. 1. Plots of the $\theta=0°$ and $\theta=90°$ $T_1$'s as a function of $\tau_c$ for the 120° jump (---) and diffusion (—) mechanisms. $\tau_c=k^{-1}$ for jumps and $D^{-1}$ for diffusion with $k$ being the jump rate and $D$ the diffusion constant.

or bond to the applied magnetic field ($\mathbf{B}_0$). So, molecular dynamics can modulate the interaction and create fluctuations that result in relaxation.

Of the different types of relaxation, the relaxation that returns a spin system from a perturbed state to equilibrium (or Zeeman magnetization) is known as spin-lattice relaxation and has a time constant, $T_1$. The spin-lattice relaxation rate is given by[3]

$$1/T_1(\omega_0,\tau_c,\ldots)=\frac{\omega_q^2}{3}[J_1(\omega_0,\tau_c,\ldots)+4J_2(2\omega_0,\tau_c,\ldots)]. \tag{1}$$

Likewise, the decay rate from a quadrupolar ordered state is given by[6,13]

$$1/T_{1Q}(\omega_0,\tau_c,\ldots)=\omega_q^2 J_1(\omega_0,\tau_c,\ldots), \tag{2}$$

where ''$\tau_c,\ldots$'' implies that the quantity is dependent on the correlation time, $\tau_c$, and other (orientational, mechanistic, etc.) variables; $\omega_0$ is the Larmor frequency; $\omega_q$ equals 3/4 the quadrupole coupling constant ($\mathrm{QCC}=2\pi e^2qQ/h$, typically 150–170 kHz for an aliphatic deuteron),[13] and, the $J_i$'s are the spectral densities, which are the Fourier transforms of their respective autocorrelation functions. The $J_i$'s can be viewed as a measure of the intensity of motion with frequency, $\omega_0$ (or $2\omega_0$), and rotational symmetry, $i$. The rotational symmetry refers to that of the first ($i=1$) and second ($i=2$) order spherical harmonics (or Wigner rotation matrices) and the motion capable of inducing single and double quantum transitions, respectively. These expressions summarize the essential features of $T_1$ and $T_{1Q}$ relaxation in that their rates are directly proportional to the magnitude of the local fields created, QCC, and the type and intensity of motion around $\omega_0, J_i$.

An aspect not evident from Eq. (1) or (2) is that plots of $T_1$ or $T_{1Q}$ vs $\tau_c$ or temperature have a minimum around $\tau_c\omega_0=1$. Generally, at this $\tau_c$, the local field fluctuations caused by molecular motion are at the same frequency as required for a transition and relaxation is most efficient. As $\tau_c$ either increases or decreases from this value (usually as a result of temperature changes), the frequencies of the fluctuations move away from $\omega_0$ and relaxation becomes less efficient ($T_1$ increases). Unless otherwise noted, we refer to slow and fast motion in relation to the minimum of Fig. 1, with slow referring to the left side of the minimum with $\omega_0\tau_c>1$ and fast to motion with $\omega_0\tau_c<1$.

Most methods for determining $T_1$ and $T_{1Q}$ monitor the decay from or return to an ordered state as a function of an experimental delay time, $t$.[18–20] Some experiments, such as inversion-recovery, monitor both. For $T_1$, Zeeman order is generated by simply allowing the deuterons to equilibrate relative to $\mathbf{B}_0$. For $T_{1Q}$, quadrupole order is usually created (and observed) with a Jenner-Broekaert type pulse sequence.[21,22] For both types of relaxation, the observed magnetization, $M_\omega(t)$, as a function of $t$ and at frequency $\omega$ can be expressed as

$$M_\omega(t)=a-bH_\omega(t), \tag{3}$$

where $a$ and $b$ depend on the experimental conditions and $H_\omega(t)$ is the fraction of intensity at $\omega$ remaining (or formed) after time $t$. Often, $a=M_\infty$, $b=(M_\infty-M_0)$, and $H_\omega(t)=\exp(-t/T_{x,\omega})$, where $M_0$ and $M_\infty$ are the magnetizations at $t=0$ and $t=\infty$, respectively, and $T_{x,\omega}$ is the relaxation time constant for the resonance at $\omega$. The subscript $x$ represents $T_1, T_{1Q}$, etc. Typically, $a$, $b$, and $T_{1,\omega}$ are simultaneously

varied to achieve the best fit of Eq. (3) to the experimental data. As an alternative to fitting Eq. (3) to the data, the scaled change in $M_\omega(t)$,

$$\{M_\omega(t_i)-M_\omega(t_j)\}/\{M_\omega(t_1)-M_\omega(t_n)\} = \{H_\omega(t_i)-H_\omega(t_j)\}/\{H_\omega(t_1)-H_\omega(t_n)\} \quad (4)$$

and/or the relative change of $M_\omega(t)$ with respect to $t$,

$$\{dM_\omega(t_i)/dt\}/\{dM_\omega(t_j)/dt\}=\{dH_\omega(t_i)/dt\}/\{dH_\omega(t_j)/dt\} \quad (5)$$

could be used. The subscripts $i$, $j$, $l$, and $n$ refer to the $i$th, $j$th, first, and last experimental point, respectively[23] and $dM_\omega(t)/dt$ refers to the derivative of $M_\omega(t)$ with respect to $t$. These equations are not dependent on experimental parameters such as $M_0$ and $M_\infty$ and emphasize that all the rate information is contained in $H_\omega(t)$.

In the solid-state deuterium powder spectra of polymers, the simple exponential decay, $H_\omega(t)=\exp[-t/\{T_{1,\omega}$ or $T_{1Q,\omega}\}]$, is usually complicated by both the orientational dependence of the relaxation rate (anisotropy)[3,13] and the heterogeneity of the systems.[15,24,25] The complications caused by the orientational dependence can be seen by examining the NMR resonance frequency[17]

$$\omega(\Theta,\phi)=\pm\omega_q/2(3\cos^2\Theta-1-\eta\sin^2\Theta\cos 2\phi), \quad (6)$$

where $\omega(\Theta,\phi)$ is relative to $\omega_0$; $\Theta$ and $\phi$ are the polar and azimuthal angles, respectively, describing the orientation of the principal axis of the efg to $\mathbf{B}_0$; $\eta$ is the asymmetry parameter which is a measure of the efg's deviation from cylindrical symmetry; and, the $\pm$ is representative of the two ''transitions'' of the deuteron. Equation (6) does not have a one to one correspondence between orientation and frequency. Thus, the magnetization at a frequency can be a superposition of different orientations with different relaxation rates and the overall $H_\omega(t)$ for a frequency will be

$$H_\omega(t)=\sum_{\Theta,\phi} w_{\Theta,\phi}\exp[-t/T_x(\tau_c,\Theta,\phi)], \quad (7)$$

where $w_{\theta,\phi}$ is the weight of each component and the sum runs over all the combinations of $\Theta$ and $\phi$ that generate a resonance at $\omega$. The sum could be expanded to account for the natural linewidth of resonances as well.

The various environments present in a solid polymer can also cause nonexponential relaxation. As a first approximation, the heterogeneity could result in a distribution of $\tau_c$'s within the sample and $H_\omega(t)$ becomes

$$H_\omega(t;\tau_m,\sigma)=\int d\tau_c\sum_{\Theta,\phi} G(\tau_c;\tau_m,\sigma)w_{\Theta,\phi} \times\exp[-t/T_x(\tau_c,\Theta,\phi)], \quad (8)$$

where $G(\tau_c;\tau_m,\sigma)$ represents the distribution and $\tau_m$ and $\sigma$ are mean and width parameters, respectively. Often, a log-normal distribution of $\tau_c$'s is used, which corresponds to a Gaussian distribution of activation energies ($E_a$)—assuming the $\tau_c$'s have an Arrhenius relation.[26] A stretched exponential form of $H_\omega(t)$ has also been used to model nonexponential relaxation.[25] This form of $H_\omega(t)$ is essentially equivalent to using the skewed distribution that results from the inverse Laplace transform of the stretched exponential.[27]

For the methyl-$d_3$ relaxation experiments investigated in this study, some simplifications of the above equations result. First, the approximate cylindrical symmetry of its efg tensor ($\eta=0$) and fast ($\tau_c<\mathrm{QCC}^{-1}$) rotation about its symmetry axis reduce $\omega(\Theta,\theta)$ for a methyl deuteron to[3]

$$\omega(\theta)=\pm\frac{\omega_q'}{2}(3\cos^2\theta-1), \quad (9)$$

where $\omega_q'=\omega_q/3$ and $\theta$ is now the angle between the symmetry axis of the methyl group and $\mathbf{B}_0$. It should be noted that although $\omega(\theta)$ is independent of $\phi$, the spectrum is still a superposition of $\phi$ values, as will be the relaxation rates if they are $\phi$ dependent. Also, although Eq. (9) has a ''reduced'' coupling parameter, $\omega_q'$, relaxation rates are still dependent on $\omega_q=3/4\,\mathrm{QCC}$.

Two mechanisms that seem to represent the experimental extremes of $T_1$ anisotropy for methyl rotation about a static symmetry axis are continuous rotational diffusion and a symmetric, 120° (three-site) jump.[3] Derived analogously to those of Torchia and Szabo,[3,28] the spectral densities for rotational diffusion, $J_{1d}(\omega,\tau_c,\theta)$ and $J_{2d}(\omega,\tau_c,\theta)$, are

$$J_{1d}(\omega,\tau_c,\theta)=4\tau_c/27[(1-3\cos^2\theta+4\cos^4\theta)/(1+\omega^2\tau_c^2) +8(1-\cos^4\theta)/(16+\omega^2\tau_c^2)], \quad (10)$$

$$J_{2d}(\omega,\tau_c,\theta)=4\tau_c/27[(1-\cos^4\theta)/(1+\omega^2\tau_c^2) +2(1+6\cos^2\theta+\cos^4\theta)/(16+\omega^2\tau_c^2)], \quad (11)$$

and those for the three-site jump, $J_{1j}(\omega,\tau_c,\theta,\phi)$ and $J_{2j}(\omega,\tau_c,\theta,\phi)$, are

$$J_{1j}(\omega,\tau_c,\theta,\phi)=4\tau_c/9[(3-3\cos^2\theta+2\cos^4\theta) -32^{1/2}\cos\theta\sin^3\theta\cos(3\phi)]/(9+\omega^2\tau_c^2), \quad (12)$$

$$J_{2j}(\omega,\tau_c,\theta,\phi)=4\tau_c/9[(3+6\cos^2\theta-\cos^4\theta)/2 +2^{1/2}\cos\theta\sin^3\theta\cos(3\phi)]/(9+\omega^2\tau_c^2), \quad (13)$$

Both $\theta$ and $\phi$ refer to the polar angles of the symmetry axis relative to $\mathbf{B}_0$. For the rotational diffusion model $\tau_c=D^{-1}$, where $D$ is the diffusion coefficient; and for the jump model, $\tau_c=k^{-1}$ where $k$ is the jump rate. With these designations, $\tau_c$ is the inverse rate constant and not the actual correlation time. The most notable difference between these models is that the three-site jump mechanism appears to be $\phi$ dependent. However, as shown in the Appendix, after integration over $\phi$ this dependence can be removed and $J_{1j}(\omega,\tau_c,\theta,\phi)$ and $J_{2j}(\omega,\tau_c,\theta,\phi)$ rewritten as

$$J_{1j}(\omega,\tau_c,\theta)=4\tau_c/9[(3-3\cos^2\theta+2\cos^4\theta)]/(9+\omega^2\tau_c^2), \quad (14)$$

$$J_{2j}(\omega,\tau_c,\theta)=2\tau_c/9[(3+6\cos^2\theta-\cos^4\theta)]/(9+\omega^2\tau_c^2). \quad (15)$$

With this modification, $H_\omega(t)$ must be multiplied by a function, $h(t;\tau_c,\theta)$, which is given in the Appendix for both $T_1$ and $T_{1Q}$. For $T_1$, $h(t;\tau_c,\theta)$ is essentially 1 for all values of $t$ in which $M_\omega(t)$ is observable and hence it can be ignored. For $T_{1Q}$, the $h(t;\tau_c,\theta)$ term should be included. The exact form of $H_\omega(t)$ with this modification will be shown below.

For these two models, $\theta$ is the only relaxation rate parameter dependent on orientation. Thus, for simplicity, $T_1$ and $T_{1Q}$ will now be subscripted by $\theta$ instead of $\omega$ to denote the relaxation rate of a resonance. The values of $\theta$ range from 0° to 90° and are related to $\omega$ through Eq. (9). Figure 1 illustrates the $T_1$ differences between the two models for the $\theta=0°$ (edge) and 90° (maxima) resonances. Because the $\theta=0°$ and 90° frequencies have the smallest and largest $T_1$ values, the curves in Fig. 1 and the corresponding ratios of $T_{1,90}$ to $T_{1,0}$ demonstrate the maximum $T_1$-$\theta$ dependence of the models. For slow rotation ($\omega_0\tau_c>1$), the models have similar $\theta$ dependencies and are difficult to distinguish with $T_1$ data. In this region, the $T_{1,90}/T_{1,0}$ ratios equal 1.5 and 1.4 for the rotational diffusion and jump models, respectively. As the reorientation rate increases and passes through the $T_1$ minimum ($\omega_0\tau_c=1$), the $T_{1,90}/T_{1,0}$ ratio for rotational diffusion first increases from 1.5 to 2.2 and then decreases to 1 in the fast motion regime ($\omega_0\tau_c<1$). For the jump model the ratio goes smoothly from 1.4 (slow) to 2 (fast). Again, the models appear too similar around the minimum to discern by $T_1$ anisotropy alone. However, when the motion is fast, the entire powder pattern relaxes at the same rate (no $\theta$ dependence) for the rotational diffusion model in contrast to the jump model which has a $T_{1,90}/T_{1,0}$ ratio of 2. This difference can be observed experimentally.

A plot of $T_{1Q}$ vs $\tau_c$ would look similar to that of $T_1$ vs $\tau_c$ in that the rates of the two mechanisms are relatively similar, but the $\theta$-dependence is different. For $T_{1Q}$, the middle region of the powder pattern, with $\theta=54.7°$, also becomes a distinguishing factor. The jump mechanism has $T_{1Q,0}:T_{1Q,54.7}:T_{1Q,90}$ ratios of 6:9:4, independent of $\tau_c$. For rotational diffusion, these ratios vary with $\tau_c$ and are 12:27:16 in the fast region. With slow diffusive motion, the $T_{1Q,54.7}$ lies between $\theta=0°$ and 90° values, as with $T_1$; however, the $\theta$-dependence is reversed, as compared to $T_1$, with the $\theta=0°$ resonance relaxing 4.5 times slower than the $\theta=90°$ resonance. The difference in these ratios makes $T_{1Q}$ experiments most suitable for distinguishing between the mechanisms in the slow motion regime.

The $T_1$ and $T_{1Q}$ behavior of the two mechanisms can be divided into that of fast ($\omega_0\tau_c<1$) and slow ($\omega_0\tau_c>1$) methyl reorientation and summarized in relation to the changes of the powder pattern with an increasing delay time, $t$. In the fast regime, $T_{1Q}$ relaxation is similar for both mechanisms with the middle region ($\theta=54.7°$) decaying the slowest. For $T_1$ in the fast regime, the rotational diffusion mechanism predicts that the entire powder pattern relaxes at the same rate and the jump mechanism predicts that the horns ($\theta=90°$) will decay twice as slow as the edges ($\theta=0°$). For slow reorientation, $T_1$ relaxation is similar for both mechanisms with the horns decaying roughly 50% slower than the edges. For $T_{1Q}$ in the slow regime, with rotational diffusion the edges will decay 4.5 times slower than the horns and, for jumps, the middle will decay roughly twice as slow as the horns or edges. Thus, without any further complications such as axis motion, the mechanisms should be distinguishable in both the fast ($T_1$) and slow ($T_{1Q}$) regimes.

Often, methyl-$d_3$ powder patterns show $\theta$-dependent relaxation behavior between that of rotational diffusion and jumping.[13,29] For reasons discussed later, we combine the mechanisms in a serial or homogeneous manner where all methyls switch between jumping and diffusing often during the experiment, but do not change their rate or $\tau_c$, as defined above. With this model each deuteron has the same average environment and an effective rate, $1/T_x(\tau_c,\theta,f)$, results from the weighted sum of the individual rates,

$$1/T_x(\tau_c,\theta,f)=f/T_{xj}(\tau_c,\theta)+(1-f)/T_{xd}(\tau_c,\theta), \quad (16)$$

where $T_x$ refers to either $T_1$ or $T_{1Q}$; the subscripts $d$ and $j$ refer to the rotational diffusion and jump mechanisms, respectively; and $f$ represents the fraction of time the deuteron jumps and is equivalent to the parameter used by Torchia and Szabo[3] to generalize their models. $T_{xd}(\tau_c,\theta)$ and $T_{xj}(\tau_c,\theta)$ are derived with the substitutions of Eqs. (7) and (9), respectively, into Eq. (1) or (2).

For this homogeneous combination model, $H_\omega(t)$ becomes

$$\begin{aligned} H_\omega(t;\tau_c,f)=&\,w_+h(t\cdot f;\tau_c,\theta_+)\exp[-t/T_x(\tau_c,\theta_+,f)] \\ &+(1-w_+)h(t\cdot f;\tau_c,\theta_-) \\ &\times\exp[-t/T_x(\tau_c,\theta_-,f)], \end{aligned} \quad (17)$$

where the $\theta_\pm$'s are the angles from the ''$\pm$'' transitions corresponding to $\omega$ [determined from Eq. (9)]; $w_+$ is the fraction of the intensity from the ''+'' transition at $\omega$ which can be calculated if the line shape is known; and, $h(t\cdot f;\tau_c,\theta)$ is the function incorporating the $\phi$ dependence with $t$ multiplied by $f$. Once again, $h(t\cdot f;\tau_c,\theta)$ is essentially 1 for $T_1$ and given by Eqs. (A5) and (A6) of the Appendix for $T_{1Q}$.

Finally, for this model of methyl reorientation, including a distribution of $\tau_c$'s results in

$$H_\omega(t;\tau_m,\sigma,f)=\int d\tau_c G(\tau_c;\tau_m,\sigma)H_\omega(t;\tau_c,f), \quad (18)$$

where $H_\omega(t;\tau_c,f)$ is the sum of only two angles, Eq. (17). Relative to Fig. 1, the distribution flattens and raises the curves as its width increases. This effect extends both the time scales associated with the minimum and the $\tau_c$ at which the models have significantly different $T_1$ and $T_{1Q}$ behavior. If the model applies, Eqs. (4)–(5) using either Eq. (17) with two parameters or Eq. (18) with three parameters should fit the relaxation behavior of the entire methyl-$d_3$ powder pattern. These fits are in contrast to using Eq. (3), which would have 3 or 4 parameters for each $\omega$. It should be noted that successful fits only suggest the validity of the model and do not prove it.

## EXPERIMENT

The synthesis and characterization of PMPS-$d_3$ was described previously.[30] For PAMS-$d_3$, trideuteromethylstyrene (AMS-$d_3$) was synthesized by reacting trideuteromethylphe-

nylketone ($PhCOCD_3$) with the ylid created from bromomethyltriphenylphosphine ($Ph_3PCH_3Br$) and NaH. DMSO was the solvent for these reactions. The AMS-$d_3$ was then polymerized in THF at $-78\,^{\circ}C$ with sec-butyllithium. The resulting PAMS-$d_3$ had a molecular mass and polydispersity of 22.7 kDa and 1.1, respectively, based on polystyrene standards. Liquid state deuterium NMR at 60.3 MHz showed that approximately 20% of the deuterons were on the backbone after the polymerization, probably resulting from the sec-butyllithium rearranging the AMS-$d_3$. Proton NMR at 200 MHz showed the polymer to be atactic.[31] Using an 8 mg sample and a heating rate of 10 °C/min, differential scanning calorimetry (DSC, TA Instruments DSC model 2010) showed a glass transition at 130 °C. This value is similar to other reported values for this molecular mass.[31] It should be noted that though a molecular mass of 22.7 kDa is relatively small, it is quite close to where $T_g$ becomes independent of molecular mass.[31]

The NMR instrumentation was the same as previously described.[30] The experiments were performed on a modified Varian VXR/S at 60.3 MHz with a 90° pulse width of 2.7 $\mu$s. For PAMS-$d_3$, the $T_1$ relaxation data was collected primarily with the solid-echo inversion-recovery sequence (IR),

$$\pi - t - \pi/2_x - \tau - \pi/2_y - \tau\,\mathrm{FID(echo)} +$$

and, for PMPS-$d_3$, a modified fast inversion-recovery sequence (FIR) was used,[20]

$$\pi - t - \pi/2_x - \tau - \pi/2_y - \tau\,\mathrm{FID(echo)} +$$

$$t - \pi/2_x - \tau - \pi/2_y - \tau\,\mathrm{FID(echo)} -$$

where the $\pm$ implies addition or subtraction of the FID's. Both sequences had 32 phase cycles. The echo delay, $\tau$, was set to 30 $\mu$s and $t$, the delay time of $M_\omega(t)$ and $H_\omega(t)$, was varied to collect 8–15 spectra. The only difference noticed between the two sequences was experimental time. The sweep width was 2 MHz for all spectra with audio filters set to 170 kHz. The FID's were left shifted to the top of the echo, zero filled to 16k data points, and convoluted with a Gaussian of 1–2 kHz before the Fourier transform. The time between scans was 150 ms for PAMS-$d_3$ and 1.75 s for PMPS-$d_3$. The scan rate for PAMS-$d_3$ was fast enough to saturate the backbone deuterons. Solid-echo spectra were acquired similarly, except with the usual eight phase-cycle pulse sequence and possibly different repetition times as noted later.

$T_{1Q}$ relaxation was measured using the sine mode of the two-dimensional exchange pulse sequence with the same parameters as previously described.[30] The sweep width, filters, relaxation delays, and Gaussian broadening were the same as the $T_1$ experiments. For the $T_{1Q}$ pulse sequence, the mixing time, $t_m$, was equivalent to the delay time, $t$.

For each temperature, the array of $T_1$ spectra was divided into 30 linearly-spaced angles according to Eq. (9). For each of the 30 angles, the 8–15 values of $M_\theta(t)$ were splined together. Twenty logarithmically $t$-spaced values of $M(t)$'s and $dM(t)/dt$ for each angle were then recovered from the splines and simultaneously fit to Eqs. (4) and (5) with $j=i+2$ and Eqs. (17) and (18) as $H(t)$. The splines smoothed the data, especially $dM(t)/dt$, and allowed consistent sampling of $M(t)$ and $dM(t)/dt$ on the $t$ scale. Fits using Eq. (6) failed to give physically reasonable results regardless of whether separate $M_0$ and $M_\infty$ values were used for each $\theta$ or scalable $M_0$ and $M_\infty$ powder patterns were used.

For the distribution, a discrete version of the log-normal distribution was sampled at 20 logarithmically spaced values of $\tau_c$. The discrete version was

$$G(\tau_c;\tau_m,\sigma) = \frac{1}{\sigma\sqrt{2\pi}}\exp[-(\ln(\tau_c/\tau_m)/2\sigma)^2], \qquad (19)$$

where $\sigma$ was essentially the half-height full-width (HHFW) (Ref. 26) in decades and $\tau_m$ was the log-average of the distribution. For the relaxation fits, both samples had the QCC set to 170 kHz. Changing the QCC by $\pm 5$ kHz did not affect the results significantly. The weights, $w_+$, were based on a static powder pattern convoluted with a Gaussian.[26] Both the ''reduced'' QCC and line broadening used in this calculation were found by fitting the experimental spectra to a theoretical pattern. In this fit, the middle region ($\pm 5$ kHz from the center) of the spectra was ignored for the low-temperature PAMS-$d_3$ spectra and when the spectra contained a central, fast-isotropic resonance. This ''reduced'' QCC was also used for the frequency-angle relation of Eq. (9). To compare the fits to the spectra, $a$ and $b$ of Eq. (2) were found by a linear least-squares fit of $M_\theta(t)$ and the fitted $H_\theta(t;\tau_m,\sigma,f)$ to the line defined by Eq. (3).

It should be noted that Eq. (9) is not valid when the methyls reorient with $\tau_c$'s greater than about $10^{-6}$ s. So, the $\theta$ dependence of this analysis is not strictly valid for the lower-temperature PAMS-$d_3$ data; however, the overall relaxation rate should still be reasonably accurate as it is primarily dependent on $\tau_c$ and not affected by the line-shape changes that occur in the intermediate region, $10^{-6} < \tau_c < 10^{-3}$ s.[24,26,29,32,33] The more severely distorted PAMS-$d_3$ spectra below $-75\,^{\circ}C$ were not used.

## RESULTS

The solid-echo spectra of PMPS-$d_3$ from $-125$ to 0 °C are unremarkable and similar to the higher temperature spectra already published.[30] They are typical of a methyl-$d_3$ quickly ($\tau_c \ll \mathrm{QCC}^{-1}$) reorienting about its symmetry axis and have a reduced splitting (distance between the maxima or horns) of about 41 kHz. The intensities of the spectra begin to decline above 25 °C as a result of backbone motion in the intermediate region ($10^{-6} < \tau_c < 10^{-3}$ s).[30] Below about $-150\,^{\circ}C$, a static pattern (splitting = 124 kHz), indicative of methyl rotation much slower than $\mathrm{QCC}^{-1}$ ($\tau_c > 10^{-4}$ s), begins to build in, superposed on the reduced pattern.

The spectra of PAMS-$d_3$ (Figs. 2 and 3) are slightly atypical of a methyl-$d_3$ group. At temperatures below 175 °C, above which isotropic backbone motion collapses the spectra, their reduced splitting is about 38 kHz or about 3 kHz less than the usual. Also, as can be seen in the low temperature spectra of Fig. 2, as temperature increases a static methyl-$d_3$ component is present until an unusually high temperature of $-50\,^{\circ}C$ and an increased central inten-

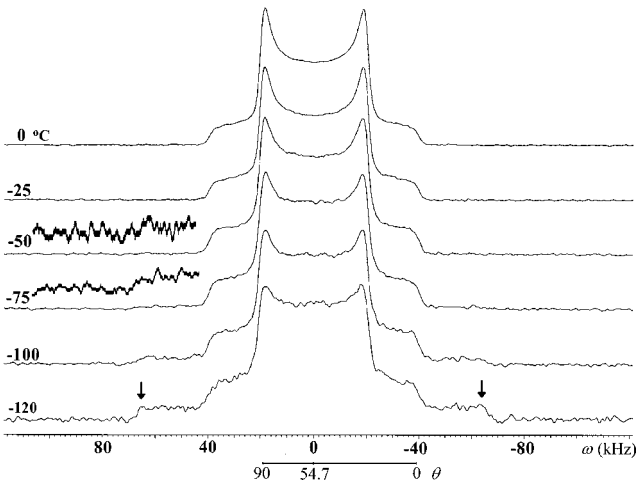


FIG. 2. Low-temperature solid-echo spectra of PAMS-$d_3$. The $\theta$ scale applies to the transition that has its horn or maxima around 19 kHz. The arrows on the $-120$ °C spectrum mark the horns of the ''frozen'' methyl powder pattern which is only evident at $-50$ and $-75$ °C as an increased baseline.

sity along with an overall loss of intensity is evident until 0 °C. The increased central intensity and loss of intensity are typical of methyl rotation in the intermediate region.[24,26,32,33] Because the relaxation delay for the spectra in Fig. 2 was 150 ms and the $T_1$ of the backbone deuterons is above 3 s, the backbone deuterons were saturated and are not visible.[34] The spectra in Fig. 2 are scaled to approximately equal heights and both the $\omega$ and $\theta$ scales are shown to illustrate their relation to the powder pattern and each other Eq. (9).

The relaxation delay for the high temperature PAMS-$d_3$ spectra of Fig. 3 was 20 s and the 90° horns of the backbone deuterons are visible as satellites about the main methyl powder pattern. Disregarding these backbone deuterons, the methyl-$d_3$ powder patterns are similar to the 0 °C spectra except for the presence of a fast-isotropic (central) resonance and intensity loss. The relative amount of the fast-isotropic resonance and the intensity loss of the spectra begin to increase significantly above 100 °C. These spectra are shown in an absolute intensity scale and are not corrected for the Boltzmann temperature dependence of the magnetization. The spectral intensities of both PAMS-$d_3$ and PMPS-$d_3$, corrected for the Boltzmann factor, are plotted in Fig. 4. In this plot, the low-temperature intensities, below $-30$ °C, of PAMS-$d_3$ do not include the intensity of ''frozen'' methyl groups and, consequently, represent lower limits.

For PMPS-$d_3$ and PAMS-$d_3$, the $T_1$'s for the horns ($T_{1,90}$'s) as a function of temperature are shown in Fig. 5. These $T_1$'s correspond to the *standard* fit, which we define as Eq. (3) with $H(t)=\exp(-t/T_1)$ and $a$, $b$, and $T_1$ fitted parameters. This figure shows that the methyl-$d_3$ reorientation of PMPS-$d_3$ approaches the minimum ($\omega_0\tau_c=1$) from the fast side ($\omega_0\tau_c<1$) as the temperature decreases and that PAMS-$d_3$ is on the slow side of the minimum ($\omega_0\tau_c>1$) below about 75 °C and above it otherwise. The plot also illustrates the large difference in $T_1$ behavior between the two relatively similar polymers. Aside from the difference in the magnitude of the $T_1$'s, PMPS-$d_3$ moves far away from the minimum with increasing temperature (400 ms at 100 °C) and PAMS-$d_3$ remains relatively close to the minimum for the entire (300 °C) temperature range (note the highly expanded scale for PAMS-$d_3$).

After noting the somewhat unexpected $T_1$ behavior of PAMS-$d_3$, $T_{1Q}$ spectra were collected at various temperatures. The $T_{1Q}$ spectra for PAMS-$d_3$ at 25 °C are shown in Fig. 6. The spectra and relaxation behavior for other temperatures are similar in that the middle ($\theta=54.7°$) decays the slowest. This aspect is *only* consistent with the jump mechanism for the slow regime spectra (<50°C). A comparison of similar spectra at $-75$ and 100 °C (not shown) also reveal that the $T_{1Q,0}$:$T_{1Q,90}$ ratio changes from about 1.4 at $-75$ °C to around 1 at 100 °C which indicates a mechanistic

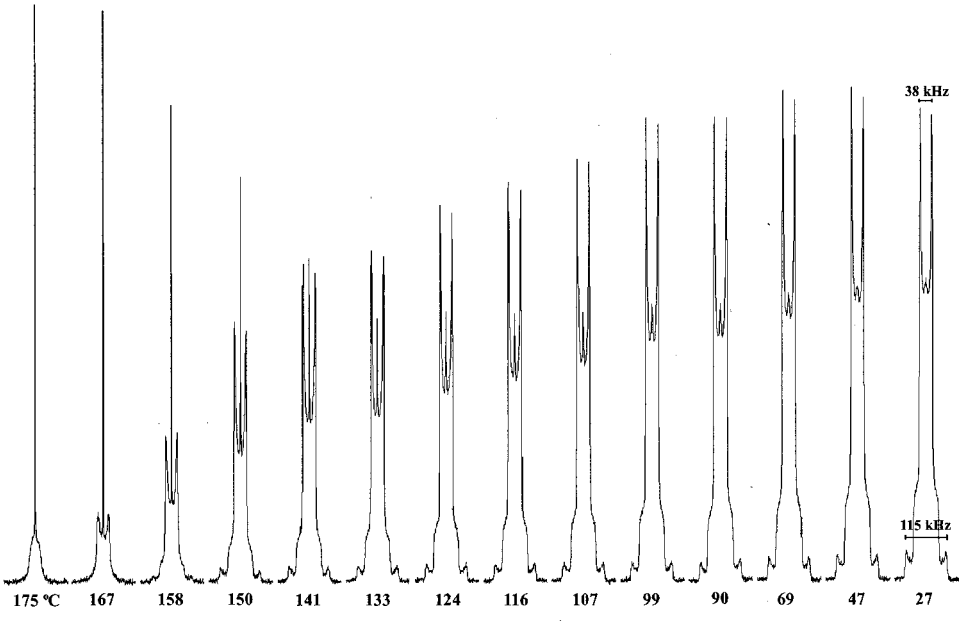


FIG. 3. High-temperature solid-echo PAMS-$d_3$ spectra. The delay between scans was 20 s and the horns of the powder pattern from backbone deuterons are also visible.

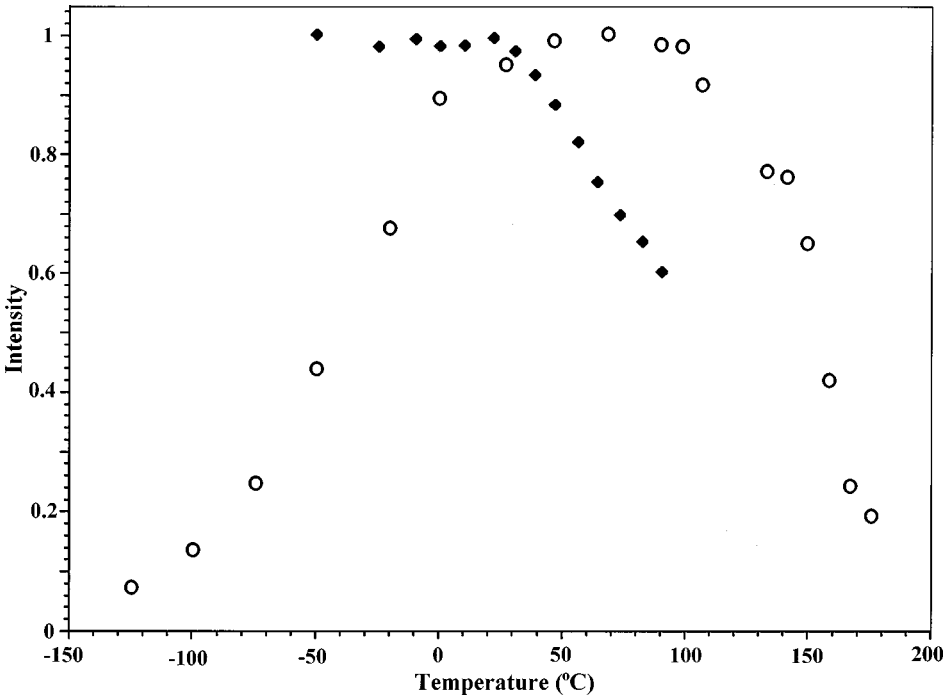


FIG. 4. Boltzmann corrected spectral intensities for PAMS-$d_3$ (○) and PMPS-$d_3$ (◆). The decrease above 100 °C for PAMS-$d_3$ and the decrease for PMPS-$d_3$ are from backbone motion. The low-temperature decrease of PAMS-$d_3$ is from intermediate region methyl rotation.

change. These ratios are based on $T_{1Q}$'s calculated from the *standard* fit. PMPS-$d_3$ $T_{1Q}$ spectra are similar in their $\theta$ dependence, but they have much higher values of $T_{1Q}$ and much lower S/N ratios. For PMPS-$d_3$, the $T_{1Q}$ spectra are somewhat unimportant as the methyl-$d_3$ group remains on the fast side of the minimum at all temperatures studied. For both polymers, the $T_1$ data alone is used to quantify the dynamic variables. The $T_{1Q}$ data are used to support and guide the analysis at lower temperatures (around the $T_1$ minimum) where the $T_1$ data can be ambiguous.

As an example of the $T_1$ spectra from the IR sequence, the array of spectra for PAMS-$d_3$ at 0 °C is shown in Fig. 7. The spectra are typical of both polymers in that the powder pattern changes slightly with increasing $t$, showing the $\theta$ dependence of the relaxation. Figure 8 shows the experimental $M(t)$ values for $\theta=90°$ of PAMS-$d_3$ at −75 °C and PAMS-$d_3$ at −125 °C. Figure 8 also has the *standard* fits, defined above, and the *model* fits [Eq. (18) with Eq. (17) as $H_\infty(t)$ and Eqs. (4)–(5) as the fitting criteria]. The *standard* fits are typical of all the data in that they decay too slowly at

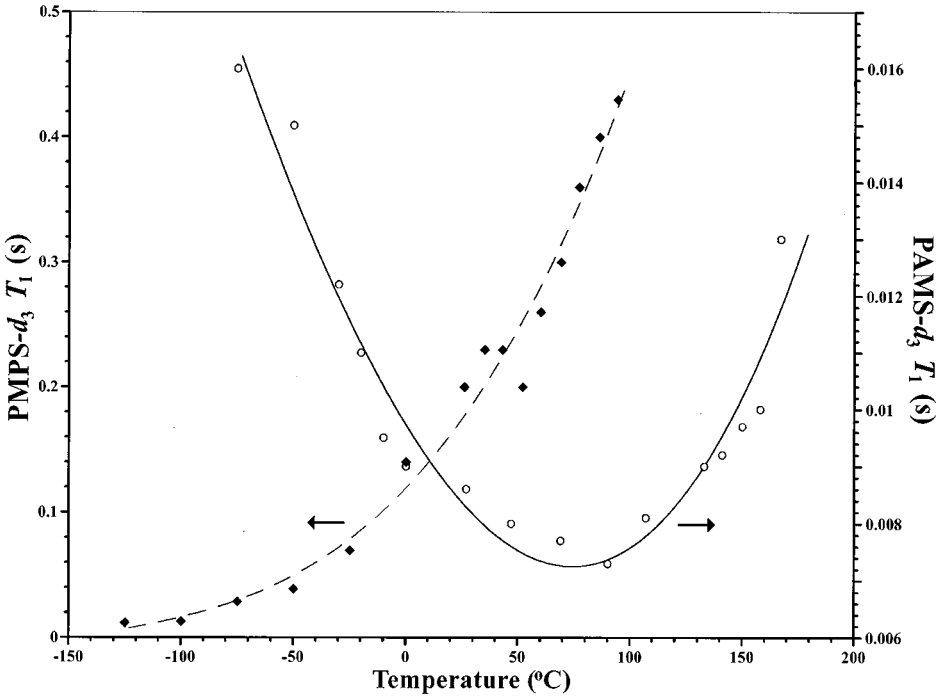


FIG. 5. The $T_1$'s from the typical three-parameter exponential fit for the $\theta=90°$ resonances of PAMS-$d_3$ (○) and PMPS-$d_3$ (◆). The curves were drawn for clarity.

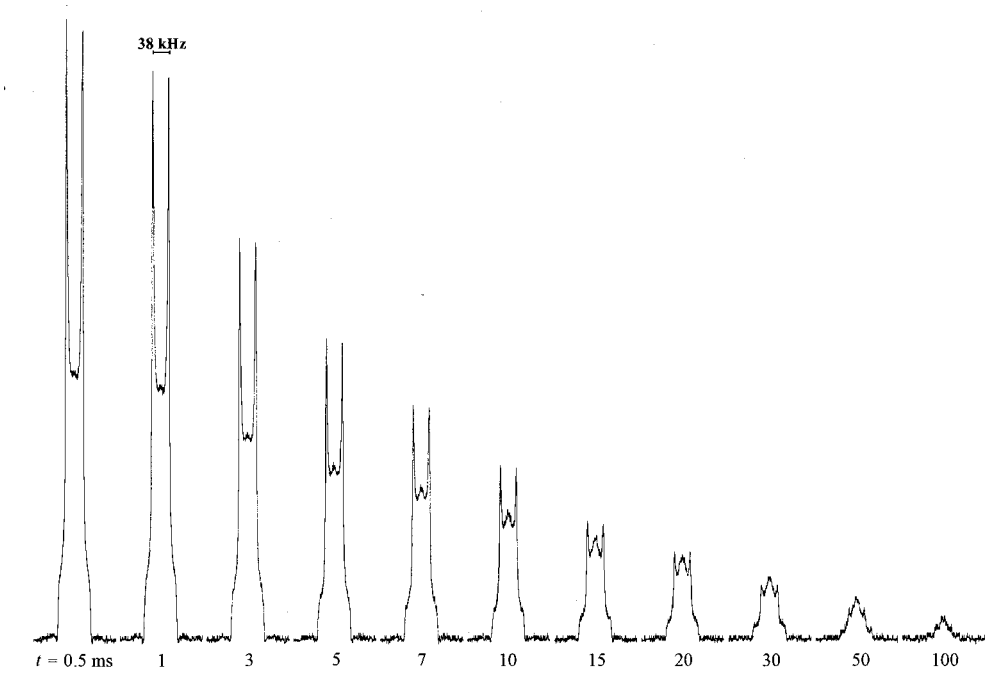


FIG. 6. $T_{1Q}$ spectra for PAMS-$d_3$ at 25 °C. Note: the middle region ($\theta = 54.7°$) relaxes the slowest.

small values of $t$ and too fast at large values. Also, from the *standard* fits, the relation between $T_1$ and $\theta$ is erratic as the inset of Fig. 8 illustrates. In general, though not necessarily evident in the inset, the $T_1$'s for the smaller angles (1°–20°) are less than $T_{1,90}$. The PMPS-$d_3$ data, with a lower S/N ratio, is more erratic than the PAMS-$d_3$ data. Allowing a $T_1$ for both $\theta$'s at a frequency [four-parameters with Eq. (7), not shown] results in even more erratic $\theta$ dependence with little decrease in fitting error.

Unlike the *standard* fits, which are typical of the data, the PAMS-$d_3$ *model* fit in Fig. 8 represents the worst *model* fit of all the data studied. Generally, like the PMPS-$d_3$ *model* fit in Fig. 8, most of the calculated points from the *model* fits are indistinguishable from the experimental data even though they force the $T_{1,\theta}$'s to a specific functional dependence of $\theta$ and have only three parameters for the entire powder pattern. Also, Eq. (17) fits (no distribution, not shown), which only account for the $\theta$-dependence, show little improvement over the *standard* fits, indicating that a distribution is necessary.

As might be expected from the plots in Fig. 1, the minimization routine behaves slightly differently with respect to initial guesses depending on whether the data is in the fast, minimum, or slow $T_1$ region. For data clearly on the fast side of the minimum, the initial guesses have little effect on the

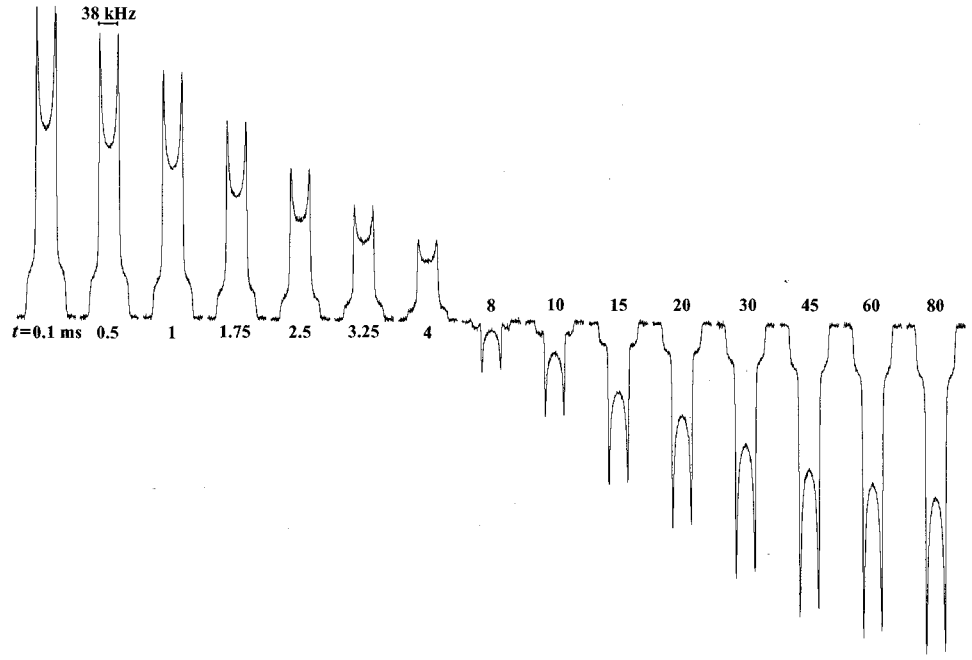


FIG. 7. A typical array of inversion-recovery spectra (PAMS-$d_3$ at 0 °C).

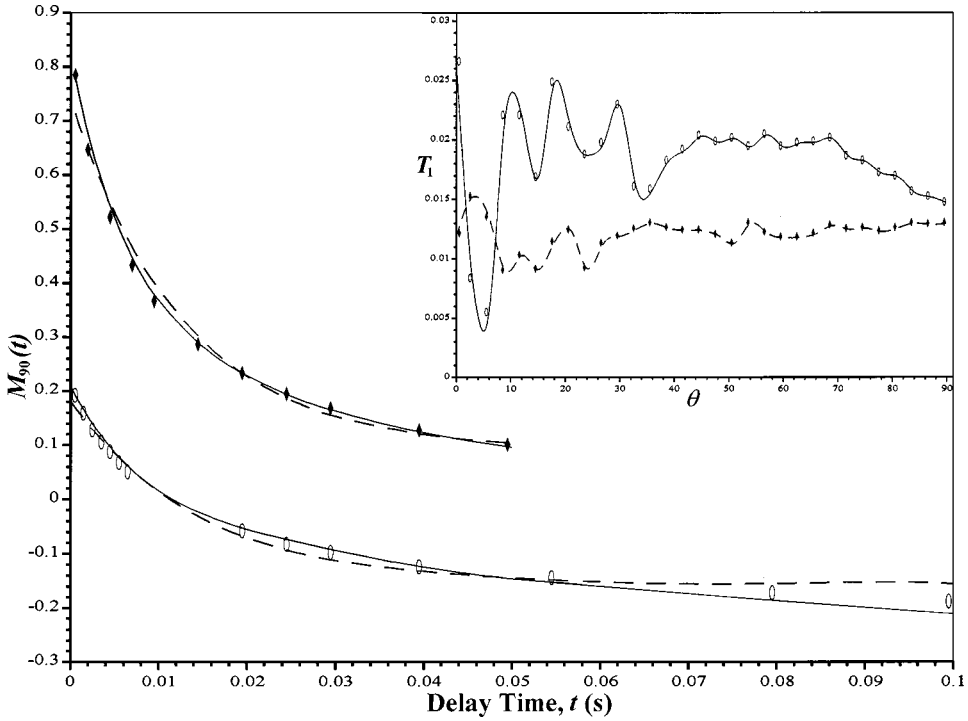


FIG. 8. Experimental points ($\theta = 90°$) and fits from the typical three-parameter fit (---) and the jump/diffusion serial model with a distribution of $\tau_c$'s (—). The $-125\,°C$ PMPS-$d_3$ data (◆) is typical of most of the data. The $-75\,°C$ PAMS-$d_3$ data (○) represent the poorest fit. The inset shows the erratic behavior the ''typical'' fit predicts for $T_1$'s as a function of $\theta$ (same temperatures and symbols).

final, converged values of the parameters $\tau_m$, $\sigma$, and $f$. Unexpectedly, the minimization routine does distinguish between the two mechanisms for the PAMS-$d_3$ data around the $T_1$ minimum—apparently, as a result of the higher $T_1$ values and larger anisotropy of the rotational diffusion model in this region (see Fig. 1). However, reasonable initial guesses of $\tau_m$ are imperative or the minimization routine tends to find local minima on either the fast or slow side of the $T_1$ minimum. Constraining $\tau_m$ to Arrhenius behavior would probably remove this difficulty, but such a constraint might also mask anomalies. With both a slightly different minimum and different $\theta$-dependence, incorporating $T_{1Q}$ data into the fitting routine might also better resolve the minimum region. For data on the slow side of the $T_1$ minimum, the parameters $\tau_m$ and $\sigma$ are well behaved as in the fast regime. However, the minimization routine behaves somewhat erratically with regard to the initial and final $f$ values. Generally, the routine converges to values of $f$ around 0.75 with reasonable initial guesses, but extreme values of any parameter could result in convergence at $f=0,1$ or even no change from its initial guess. The final values reported result from initial guesses of $f=0.75$ and $\tau_m$ and $\sigma$ equal to their average converged values. The $T_{1Q}$ spectra support this initial value of $f$ and, if incorporated into the minimization routine, the uncertainty in $f$ on the slow side of the minimum would probably be reduced. In general, the error bars for each parameter are estimated to be about $\pm 10\%$ for $\sigma$, $\pm 20\%$ for $f$, and $\pm 60\%$ for $\tau_m$. These errors are based on the range of converged values generated from different initial guesses. The large error in $\tau_m$ is somewhat misleading as it affects the fits on a log scale.

For both samples, the fitted values of the three parameter, $\tau_m$, $\sigma$, and $f$, in relation to temperature are plotted in Figs. 9, 10, and 11, respectively. The $\tau_m$'s in Fig. 9 follow Arrhenius behavior and correspond to activation energies, $E_a$, of $12 \pm 0.5$ and $4.7 \pm 0.1$ kJ/mol for PAMS-$d_3$ and PMPS-$d_3$, respectively. The $\tau_\infty$ values of the Arrhenius equation are about $6 \times 10^{-13}$ s for both samples. As can be seen from the plots, the behavior of both polymers is for an increase in both the width of the distribution, $\sigma$, and jump like reorientation, $f$, as temperature decreases. For the lower temperature PAMS-$d_3$ data, the $\sigma$'s are probably a lower limit as the ''frozen'' methyls were not part of the analysis.

## DISCUSSION

One of the main objectives of this work is to quantify the temperature dependence of the methyl dynamics. As temperature increases, this dependence is experimentally observed as a change in the magnitude of $T_1$ and a decrease in both the nonexponential character and the $T_1$ anisotropy of the relaxation. Within our model and generally, the changes in the magnitude of $T_1$ for both polymers are consistent with an increasing reorientation rate, quantified by $\tau_m$, as temperature increases. This rate increase is expected for thermally activated processes and conforms to an Arrhenius relation for both polymers. The $\tau_m$ data from PAMS-$d_3$ is consistent with dynamic mechanical analysis (DMA) which shows a 1 Hz methyl reorientation at $-160\,°C$ and an $E_a$ of 14 kJ/mol.[35] Using the $\tau_m$ vs temperature data of this study, we predict a 1 Hz jump rate at $-170\,°C$ and an $E_a$ of 12 kJ/mol. We could not locate similar data to corroborate our PMPS-$d_3$ analysis.

Because the heterogeneous morphology of polymers leads to various backbone and sidegroup environments, polymer dynamics are often modeled with distributions of reorientation rates.[15,24–26,29] For both PMPS-$d_3$ and PAMS-$d_3$, the superposition of ''frozen'' and fast-rotating methyl powder spectra at low temperatures along with their intensity

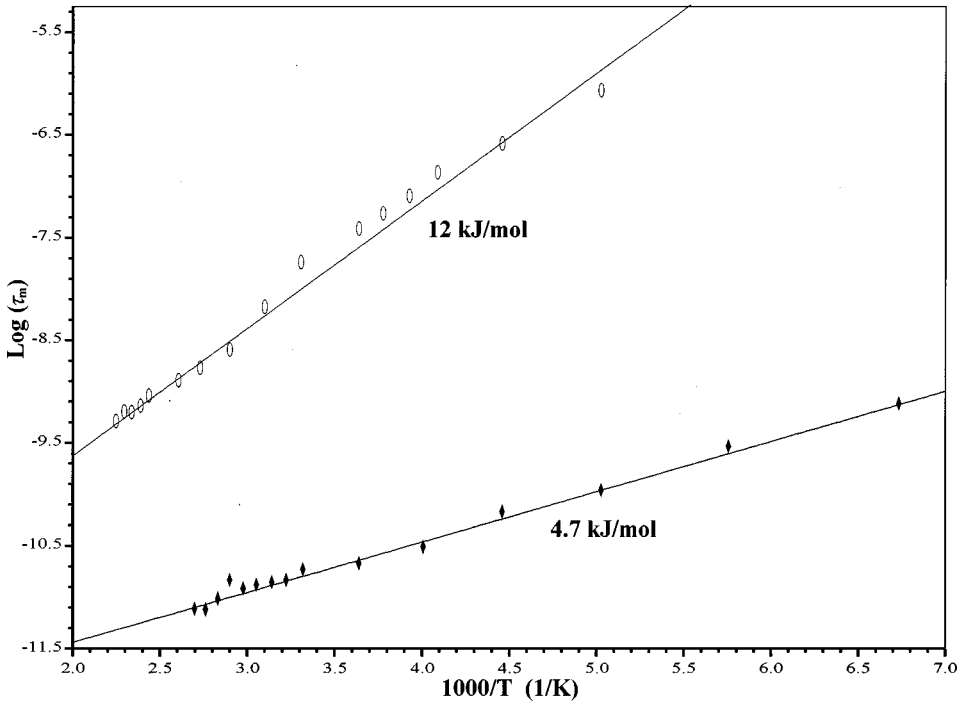


FIG. 9. The $\tau_m$'s or log-average $\tau_c$'s fit from the serial jump/diffusion model with a distribution of $\tau_c$'s as a function of inverse temperature for PAMS-$d_3$ (○) and PMPS-$d_3$ (♦). The lines correspond to Arrhenius relations.

reductions indicate a distribution of reorientation rates. Therefore, we attribute the decrease in the nonexponential character of the relaxation to a corresponding decrease in the width of the distribution of reorientation rates. The trend of increasing width as the motion slows is similar to trends in backbone dynamics where the distributions also generally broaden as the motion slows (as $T_g$ is approached from higher temperatures).[26]

The temperature dependence of the $T_1$ anisotropy (or $\theta$-dependence) of the relaxation for both polymers is, generally, between the two mechanisms of rotational diffusion and jumps. As mentioned, the relaxation becomes less anisotropic as temperature increases. In our analysis, we quantify the anisotropy with the parameter $f$ which ranges from 0 to 1 implying no $\theta$-dependence (rotational diffusion) or that of the three-site jump, respectively. Aside from the model,

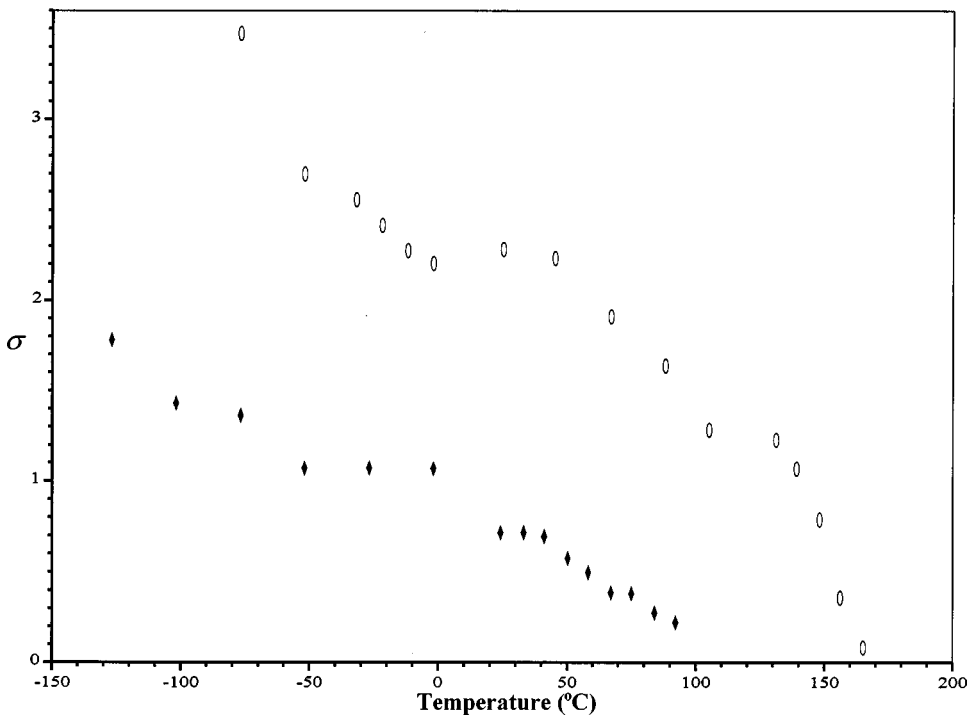


FIG. 10. The width parameters of the log-normal distribution as a function of temperature for PAMS-$d_3$ (○) and PMPS-$d_3$ (♦).

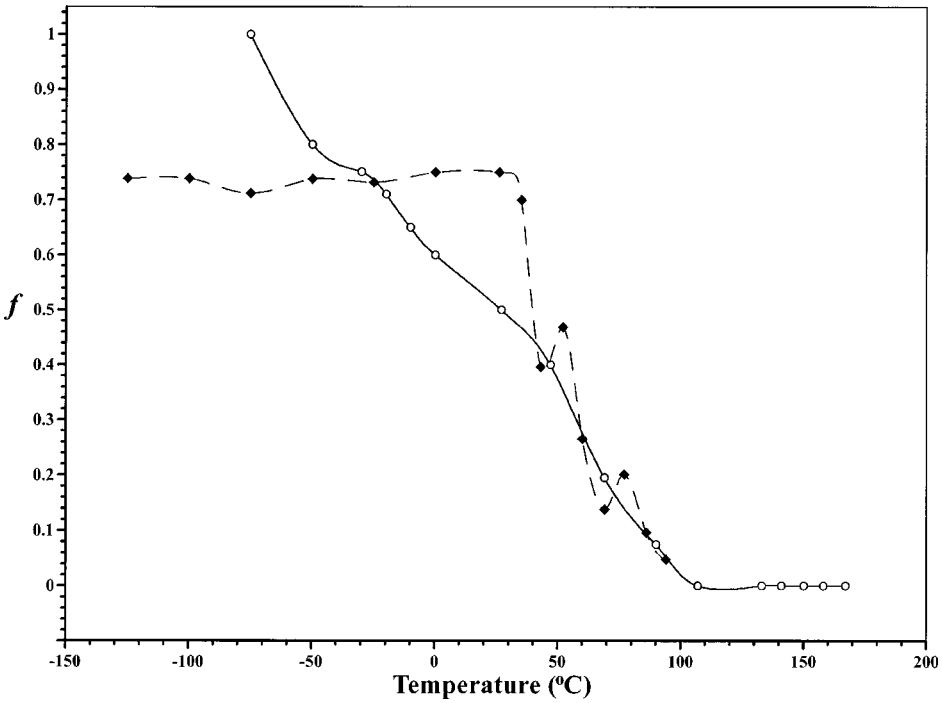


FIG. 11. The $f$ parameters of the serial jump/diffusion model representing the relative amount of time spent jumping vs diffusing as a function of temperature for PAMS-$d_3$ (○) and PMPS-$d_3$ (◆). The lines are drawn for clarity.

there are several other possible explanations for this behavior. Perhaps the simplest is that neither the jump nor the diffusion mechanisms adequately describe the methyl reorientation. Based on a Smoluchowski process, the more ''realistic'' and complicated threefold potential mechanism for methyl rotation has a $\theta$-dependence between the two mechanisms.[8] In fact, setting $f$ to around 0.75 mimics the $\theta$-dependence of the potential model in the fast regime.[3] Generally, mechanisms that have only one, fixed mode of motion, such as the three-site jump, rotational diffusion, or threefold potential, have a fixed $\theta$-dependence (independent of $\tau_c$) once $\tau_c$ is in either the fast or slow regime. In relation to PMPS-$d_3$, a refined mechanism may account for the low temperature value of $f$. However, such a mechanism alone can not explain the decrease in the $\theta$-dependence for either the fast regime PMPS-$d_3$ or PAMS-$d_3$ data. So, a *simple* refinement of the methyl rotation mechanism does not appear to be adequate.

Motion of the methyl symmetry axis could also result in a mixed $\theta$-dependence. For example, if the axis reorients by isotropic rotational diffusion (IRD) as described by a Fokker–Planck diffusion equation,[36–38] the $\theta$ dependence vanishes and the entire powder pattern relaxes at the same rate. Though this description is not applicable to a slowly reorienting axis as might occur in solids, it does serve to demonstrate the averaging of the anisotropy that can occur if the axis encounters all values of $\theta$. For solids, IRD is better described by nearest-neighbor small-angle jumps.[32] With this description, the axis does not necessarily isotropically reorient within the time frame of the experiment and there may be only partial averaging. As temperature increases, the amount that the axis reorients is likely to increase which would decrease the anisotropy.

Heterogeneous and/or fluctuating environments would also be observed as a mixed $\theta$-dependence. For example, if a fraction of the methyls are diffusing and the others are jumping (heterogeneous environments or parallel processes), $H_\omega(t)$ would be a weighted sum of exponentials from each mechanism. Or, if the mechanism switches between jumping and diffusing (serial process) often during the experiment, perhaps as a result of environmental fluctuations, $H_\omega(t)$ would be a single exponential with a time constant that is a weighted sum of the different relaxation rates, Eq. (16). For a serial process, the weights would be proportional to the time spent in each mode. Both the parallel and serial models would result in an average anisotropy and temperature changes could reasonably affect the weights and extent of averaging.

The actual dynamics of methyl groups attached to a polymer backbone are governed by a potential that is correlated with other motion, free volume, conformations, packing, etc. Considering these complications along with the average nature and limited precision of relaxation data, the serial jump/diffusion process seems a reasonable and simple approximation to the microdynamics of the methyl group. The parameter of the serial model directly quantifies changes in the local environment or potential. In contrast, the parameter of the similar parallel model quantifies the long-range heterogeneity of the system. The serial model coupled with a distribution of $\tau_0$'s attempts to separate these local and long-range effects. Additionally, in the limit of small molecules or crystals the serial model is physically more reasonable than the parallel process as it does not require heterogeneity to account for a mixed $\theta$-dependence. The actual physical picture is not the major theme, though. The purpose of the model is to quantify the change in the $T_1$ anisotropy from the slow to the fast region in a physically reasonable and straightforward manner.

Additional information is required to explain the changes quantified by $f$ of the serial model. Ignoring the

small central fast-isotropic resonance, two dimensional exchange (2D-X) NMR shows that the axis in PAMS-$d_3$ are stationary until about 130 °C.[39,40] This result is also consistent with a $T_g$ of 130 °C. So, for PAMS-$d_3$ the trend in $f$ is not due to axis motion and seems to represent a gradual mechanistic change. The relatively high temperature (−50 °C) in which the methyl rotations ''freeze'' out, high $E_a$ (12 kJ/mol), and small $T_1$'s or relatively slow reorientations suggest that the methyls in PAMS-$d_3$ have restricted environments. A recent study also suggests that PAMS-$d_3$ has slower methyl motion than other polymer methyl groups.[41] The reduced splitting of 38 kHz may also support restricted environments if the reduction results from a compressed bond angle. A change of about 1° in either the bond angle or $z$-axis of the efg could account for the reduction. With these restricted environments, a possible cause of the changes in $f$ might be phenyl reorientations. DMA studies report two phenyl reorientations beginning (1 Hz) at −104 and −38 °C with $E_a$'s of 32 and 45 kJ, respectively.[35] The first reorientation should reach 1 kHz at around −30 °C which should be fast enough to significantly affect the potential and the ''time'' a methyl group either jumps or diffuses. Thus, for PAMS-$d_3$, it seems likely that the trend in $f$ is due to phenyl motion affecting the methyl environments.

For PAMS-$d_3$ the changes also seem to result from a change in the methyl reorientation mechanism, but they are complicated by motion of the symmetry axis. Above 50 °C, 2D-X NMR indicates that the sample consists of methyl groups whose symmetry axis is either static, reorienting slowly, or reorienting fast and isotropically.[30] From these experiments, we estimate that at most from about 15% at 56 °C to 36% at 90 °C of the axis will be reorienting fast enough to significantly change the position of the axis and affect the $T_1$ anisotropy.[42] Using these percentages, the axis motion alone cannot account for the changes in $f$, but its relatively sharp decrease above 50 °C may be in part due to this motion. Because the $T_1$'s and $E_a$ of PMPS-$d_3$ are typical of methyl groups, without further information the source of the apparent mechanistic change is unknown. Plausibly, free volume increases or, with the similarity of the polymer to PAMS-$d_3$, phenyl motions may drive the change.

## CONCLUSIONS

To maximize the information and precision of the relaxation experiments, we use the entire solid-echo spectra in our analysis.[43] Additionally, the analysis is based on relationships that depend only on the relaxation and not on experimental parameters such as $M_\infty$ and $M_0$. For methyl rotation, we find $T_1$ and $T_{1Q}$ data important for motion that is faster and slower, respectively, than the Larmor frequency.

The serial model coupled with a distribution of $\tau_c$'s quantifies methyl dynamics with only three parameters—$\tau_m$, $\sigma$, and $f$, which are the log-average $\tau_c$, HHFW base 10 width (essentially) of a log-normal distribution of reorientation rates, and anisotropy of the relaxation, respectively. The anisotropy parameter $f$ is based on a serial process in which a methyl deuteron changes between the mechanisms of rotational diffusion and a three-site jump. Because these parameters have general physical meanings, this approach seems to be a compromise between the model-free approach of Lipari and Szabo[12] where ''moment'' parameters quantify the data and the generalized stochastic model of Lindenburg and Cukier.[4]

Relaxation data from two relatively similar polymers PAMS-$d_3$ and PMPS-$d_3$ are analyzed in terms of this model. Generally, at similar temperatures, the methyls of PAMS-$d_3$ reorient at least 100 times slower than those of PMPS-$d_3$. For both polymers, as temperature increases $\tau_m$ and $\sigma$ decrease, resulting in $E_a$'s of 12 and 5 kJ/mol for PAMS-$d_3$ and PMPS-$d_3$, respectively. Also, a change in $f$ or the methyl reorientation mechanism is observed for both polymers. With the aid of other data, it seems likely that the PAMS-$d_3$ methyls have restrictive environments that are closely coupled to phenyl reorientation and that phenyl reorientation faster than about 1 kHz results in diffusive methyl rotation. PMPS-$d_3$ may be similar; however, without specifically incorporating axis motion and knowing the other dynamics, the nature of the $T_1$ anisotropy is less certain and only the total anisotropy is quantified.

## ACKNOWLEDGMENT

The authors thank the National Science Foundation under Grant No. DMR9807696 for financial support.

## APPENDIX

If Eqs. (12) and (13) are substituted into Eq. (1) and then Eq. (1) into Eq. (7),

$$H_\omega(t)=\sum_\theta w_\theta \int (2\pi)^{-1} \exp[-t/T_{1j}(\tau_c,\theta,\phi)]d\phi, \quad \text{(A1)}$$

where we have replace the sum over $\phi$ with an integral and $\phi$-dependent weights with $(2\pi)^{-1}$. After separating $T_{1j}$ into $\phi$-dependent and $\phi$-independent parts Eq. (A1) can be rewritten as

$$H_\omega(t)=\sum_\theta w_\theta h(t;\tau_c,\theta)\exp[-t/T_{1j}(\tau_c,\theta)], \quad \text{(A2)}$$

where $T_{1j}(\tau_c,\theta)$ is Eqs. (14) and (15) substituted into Eq. (1) and $h(t,\tau_c,\theta)$ is the function referred to in the text and equals

$$h(t;\tau_c,\theta)=\frac{1}{2\pi}\int_0^{2\pi} \exp[t\cdot g(\tau_c,\theta)\cos 3\phi]\cdot d\phi, \quad \text{(A3)}$$

where for $T_1$,

$$g(\tau_c,\theta)=[16\omega_q^2\tau_c^2\omega_0^2 2^{1/2}\cos\theta\sin^3\theta]/ [9(9+\tau_c^2\omega_0^2)(9+4\,\tau_c^2\omega_0^2)] \quad \text{(A4)}$$

with all variables and constants defined as in the text. The integral in Eq. (A3) can be evaluated analytically and $h(t;\tau_c,\theta)$ is equal to $I_0[t\cdot g(\tau_c,\theta)]$, where $I_0$ is a Bessel function of imaginary argument, i.e.,

$$h(t;\tau_c,\theta)=I_0[t\cdot g(\tau_c,\theta)]=\sum_{k=0}^{\infty}\frac{[t\cdot g(\tau_c,\theta)]^{2k}}{(k!)^2}. \quad \text{(A5)}$$

For $T_{1Q}$ a similar procedure produces a $g(\tau_c,\theta)$ of

$$g(\tau_c,\theta)=[16\omega_q^2\tau_c 2^{1/2}\cos\theta\sin^3\theta]/[9(9+\tau_c^2\omega_0^2)]. \quad \text{(A6)}$$

As stated earlier, $h(t;\tau_c,\theta)$ using Eq. (A4) for $T_1$ is essentially 1 for all observable values of $t$. For $T_{1Q}$, however, $h(t;\tau_c,\theta)$ using Eq. (A6) should be included. Using Eq. (10) for $T_1$ instead of Eq. (1) simply results in scaling $t$ by $f$, i.e., $h(t\cdot f;\tau_c,\theta)$.


[1] A. Schleicher, K. Mueller, and G. Kothe, J. Chem. Phys. **92**, 6432 (1990).
[2] R. J. Witterbort and A. Szabo, J. Chem. Phys. **69**, 1722 (1978).
[3] D. A. Torchia and A. Szabo, J. Magn. Reson. **49**, 107 (1982).
[4] K. Lindenburg and R. Cukier, J. Chem. Phys. **62**, 3271 (1975).
[5] P. Born and T. Bluhm, J. Magn. Reson. **83**, 494 (1989).
[6] J. Hirschinger and A. D. English, J. Magn. Reson. **85**, 542 (1989).
[7] R. R. Vold and R. L. Vold, J. Chem. Phys. **88**, 1443 (1988).
[8] O. Edholm and C. Blomberg, Chem. Phys. **42**, 449 (1979).
[9] A. Tsutsumi, Mol. Phys. **37**, 111 (1979).
[10] T. Bluhm, Mol. Phys. **47**, 475 (1982).
[11] D. Kevelson and T. Keyes, J. Chem. Phys. **57**, 4599 (1972).
[12] G. Lipari and A. Szabo, J. Am. Chem. Soc. **104**, 4546 (1982).
[13] G. L. Hoatson and R. L. Vold, NMR Basic Prin. Prog. **32**, 1 (1994).
[14] H. G. Hertz, Prog. NMR Spectrosc **16**, 115 (1983).
[15] L. W. Jelinski, Annu. Rev. Mater. Sci. **15**, 359 (1985).
[16] H. Sillescu, Adv. Mol. Relax. Processes **3**, 91 (1972).
[17] A. Abragam, *Principles of Nuclear Magnetism* (Oxford University Press, Oxford, 1961).
[18] R. Freeman, H. D. W. Hill, and R. Kaptein, J. Magn. Reson. **7**, 82 (1972).
[19] T. K. Leipert and D. W. Marquardt, J. Magn. Reson. **24**, 181 (1976).
[20] A. Roscher, L. Emsley, and C. Roby, J. Magn. Reson., Ser. A **118**, 108 (1996).
[21] S. Wimperis and G. Bodenhausen, Chem. Phys. Lett. **132**, 194 (1986).
[22] H. W. Spiess, Annu. Rev. Mater. Sci. **21**, 131 (1991).
[23] Equation (4) uses the total change, $M_\omega(t_1)-M_\omega(t_n)$, as the scaling criteria and may unduly weight the first and last points. This criteria could be replaced by the average change in $M_\omega(t)$.
[24] K. J. Schmidt, K. J. Kuhn, and H. W. Spiess, Prog. Colloid Polym. Sci. **71**, 71 (1985).
[25] A. Narayanan, J. S. Hartman, and A. D. Bain, J. Magn. Reson., Ser. A **112**, 58 (1995).
[26] K. Schmidt-Rohr and H. W. Spiess, *Multidimensional Solid-State NMR and Polymers* (Academic, London, 1994).
[27] Because $T_1(\tau_c;\Theta,\phi)$ is often either directly or inversely proportional to $\tau_c$, the integral in Eq. (8) is essentially a Laplace transform.
[28] The angle between the symmetry axis of the methyl group and the bond vector was set to 70.5°.
[29] M. Wann and G. S. Harbison, J. Chem. Phys. **101**, 231 (1994).
[30] R. D. O'Connor, F. D. Blum, E. Ginsburg, and R. D. Miller, Macromolecules **31**, 4852 (1998).
[31] R. W. Lenz, J. Macromol. Sci. A **9**, 945 (1975).
[32] H. Sillescu, J. Chem. Phys. **54**, 2110 (1971).
[33] A. J. Vega and Z. Luz, J. Chem. Phys. **86**, 1803 (1987).
[34] The backbone deuterons have a $T_1$ around 3 s at 75 °C that increases as temperature decreases.
[35] G. M. Bartenev, V. V. Tulinova, and G. D. Danilenko, Vysokomol. Soedin., Ser. B **34**, 6 (1992).
[36] D. L. Favro, Phys. Rev. **119**, 53 (1960).
[37] Here, slowly refers to $\tau_c$'s$>10^{-3}$ s. This isotropic rotational diffusion applies to diffusion as described by a Fokker–Planck-type diffusion equation which is generally typical of ''liquidlike'' motion. In fact, because of the $\delta_{aa'}$, and $\delta_{bb}$, terms in the correlation function of the axis (see Ref. 38), this particular model has no $\theta$-dependence regardless of the rate the axis motion.
[38] D. Wallach, J. Chem. Phys. **47**, 5258 (1967).
[39] R. D. O'Connor and F. D. Blum (in preparation).
[40] The intensity loss between 100 and 130 °C probably results from small angle wobbling.
[41] J. L. White, Solid State Nucl. Magn. Reson. **10**, 79 (1997). Also, this study suggests that poly(4-methylstyrene) is slower than PAMS by an order of magnitude. If this is the case, poly(4-methylstyrene) should show ''frozen'' methyls at room temperature.
[42] The fast-isotropic fraction is predominantly observed as a central resonance (0 Hz) and lost intensity. It is not part of the analysis. For complete isotropic reorientation of the slowly reorienting methyls (the exchanging fraction in 2D-X NMR), the $\tau_c$ of the axis needs to be approximately 100 times the relaxation delay time, $t$. The effective percentages are approximated based on an average delay time (taken as the $T_1$ for that temperature) and the intensity of the exchange distribution with $\tau_c$'s 10 times less than the average delay time.
[43] G. L. Hoatson, R. L. Vold, and T. Y. Tse, J. Chem. Phys. **100**, 4756 (1994).